# Nonlinear Free-surface Flow Computations for Submerged Cylinders

D. Scullen and E. O. Tuck

Applied Mathematics Department
University of Adelaide

Revised version, January 1995

**Summary**

A numerical method involving isolated sources located outside the flow domain is used to compute potential flows in two dimensions involving the nonlinear water-wave boundary condition. The method is tested on Stokes waves, and then used on steady streaming flows about submerged cylinders. The circular cylinder with and without circulation is discussed for a range of submergences and Froude numbers. Emphasis is placed on the special choices of circulation for which the net vertical force is small and the amplitude of downstream waves is reduced.

## 1. Introduction

The physical problem of interest here is the determination of the steady waves that appear downstream of a body held fixed in a uniform flow, or equivalently, the waves that appear behind a body moving through calm water. For our purposes, it is convenient to consider the situation from a frame of reference that is at rest with the body.

In the present paper, we confine attention to submerged two-dimensional bodies, but use numerical methods that are capable of generalisation to three-dimensional submerged or surface piercing bodies. Specifically, we study the submerged circular cylinder with and without circulation.

The submerged circular cylinder in a steady stream of infinite depth without circulation is a very old problem. Early solutions were for deeply submerged bodies, i.e. for small ratios of cylinder radius to submergence depth. In that limiting case, the flow near the cylinder is unaffected by the free surface, and hence can be represented by a (Rankine) dipole of known strength and a line vortex of arbitrary circulation, both placed at the centre of the circle, in a uniform stream of fluid which is of apparently unlimited extent in all directions. On the other hand, in the neighbourhood of the free surface, the leading-order flow is that for the same dipole-vortex combination, but now each is submerged beneath a (Kelvin) free surface linearised for small departures from the undisturbed plane surface, for which the solution is well-known (Wehausen and Laitone 1960).

Havelock (1926) attempted to find second-order corrections to this linearised result (in the absence of circulation) by modifying the dipole singularity structure in order to more accurately satisfy the boundary condition on the cylinder. However, this does not provide a consistent second-order theory, since it is also necessary to simultaneously correct for nonlinear free surface effects. This was done (still with no circulation) by Tuck (1965). The

deep-submergence problem does not seem to have been studied with nonzero circulation.

Circulation is particularly interesting in this problem since (Tuck and Tulin 1992) it is apparently capable of cancelling the trailing wave pattern. In fact, in the first-order linearised theory, the trailing wave amplitude is a linear function of the circulation, vanishing at an anticlockwise value of circulation that generates a negative lift of exactly twice the buoyancy of the circular cylinder. One motivation of the present study is to examine the extent to which nonlinear effects alter this conclusion.

The present study never assumes small departures from a plane free surface. It is part of a more general program for nonlinear free-surface solution using techniques similar to those developed for ship wave resistance computations by Jensen et al (1986), Raven (1992), and others. The full nonlinear free-surface boundary conditions are used, but the problem is solved by a Newton-like iterative process. In that process, the free surface location is progressively refined from iteration to iteration, a special linear but nonconstant-coefficient "updating" boundary condition being applied at each step, on a temporarily fixed boundary at the previous free-surface location. As part of the present study we establish in a general and consistent manner the correct form of this updating condition in order that the iteration proceed in a quadratically convergent Newton-like manner.

The actual numerical methods used in this paper are similar to those in the above mentioned ship-hydrodynamic studies, and in particular use desingularised isolated source distributions. Since these very efficient methods have not been used on pure periodic wave-like problems before, we first give a numerical treatment of the periodic Stokes-wave problem, yielding waves of up to steepness 0.1404 without difficulty.

The method is then used on the circular cylinder without circulation. For sufficiently small radius/submergence, the linearised theory is confirmed, as is the second-order theory of Tuck (1965). In fact, the latter theory seems to be quite accurate up to close to the limiting configurations beyond which no solutions can be found.

At any fixed radius/submergence ratio, the wave amplitude (and hence wave resistance) possesses a maximum as a function of Froude number based on submergence. When that maximum is sufficiently low, linearisation is justified, and converged results in agreement with the consistent second-order theory are obtained for all Froude numbers. However, as the radius/submergence ratio is increased, that maximum wave amplitude increases until nonlinear effects are very strong, and eventually the largest crest (nearest to the cylinder) in the generated wave is nearing stagnation height. This happens at about a radius/submergence of 0.2, when there is a small range of Froude numbers around 0.7 where our program fails to converge, and where we believe there is no steady potential solution. For larger radius/submergence ratios, the range of Froude numbers where no solution is obtained widens.

When (anticlockwise) circulation is included, the downstream waves are reduced in amplitude, although the local disturbance is increased. The local free surface takes the shape of a large and wide hump with the downstream waves superimposed on it. This hump does not in itself affect the wave resistance, but it does produce a down-force on the submerged body. The wave resistance can be substantially reduced, due to the smaller amplitude of the resulting downstream waves. Some interesting results are found for non-linear disturbers.

## 2. Mathematical Formulation

### 2.1 Statement of the problem

Our objective is to determine the steady flow created by the body. We assume that the fluid is inviscid and incompressible, and the flow irrotational, which enables us to use a velocity potential $\phi$, and we restrict ourselves to two-dimensional space at this stage. Mathematically then, we are required to solve the Laplace equation in the region $R$ occupied by the fluid, subject to the usual conditions that the flow is tangential to both the free surface and the body $B$ (the kinematic conditions), and that the pressure is constant on the free surface $F$ (the dynamic condition).

Specifically, these conditions are thus

$$\nabla^2\phi = 0 \quad \text{in } R \tag{1}$$

$$\frac{\partial\phi}{\partial n} = 0 \quad \text{on } F \tag{2}$$

$$\frac{\partial\phi}{\partial n} = 0 \quad \text{on } B \tag{3}$$

$$\text{and} \qquad p = 0 \quad \text{on } F \tag{4}$$

where $p$ is the excess pressure above atmospheric, and is determined from $\phi$ by Bernoulli's equation.

Equations (1–4) do not determine a unique solution. There is in fact a two-parameter family of solutions. The most general solution corresponds to the body being submerged in a fluid that already has a wavy surface, perhaps produced by some other disturbance far upstream, so that both sets of waves move downstream at the same rate as the stream. Consequently the family of solutions can be characterised by two parameters — the amplitude of the already existing surface waves, and their phase relative to the waves produced by the body. It is not surprising then that two additional conditions are required to uniquely determine a solution. The solution that we seek is the one for which waves do not exist far upstream of the body. These conditions are usually described collectively as the "radiation condition". These two additional conditions could be any two conditions that cannot be simultaneously satisfied by the combination of a wavy free surface and the disturbance. They will be discussed again later.

The problem as stated is difficult to solve for two main reasons. The dynamic condition is non-linear in the potential $\phi$, and the location of the free surface (on which this condition must be satisfied) is unknown. A systematic approach to solving these equations is to iterate between solving for the flow beneath an approximate free surface, and using the calculated flow to determine a better approximation to the true free surface. This continues until we determine the exact free surface on which both dynamic and kinematic boundary conditions are satisfied.

### 2.2 Iteration Scheme

Let $E = 0$ be the kinematic and $P = 0$ the dynamic free-surface boundary condition. In principle these are quite general quantities, but for example, in a two-dimensional problem $E$ could be proportional to the streamfunction, and $P$ to the pressure $p$. Both $E = E(x, y)$ and $P = P(x, y)$ are functions of the space co-ordinates. Their values, however, depend implicitly on the flow via the velocity potential $\phi(x, y)$.

Our task is to find a potential $\phi(x, y)$ (satisfying Laplace's equation) and a free-surface shape $y = \eta(x)$ such that both $E = 0$ and $P = 0$ on $y = \eta$. This is a difficult nonlinear free boundary problem. Let us approach its solution by iteration in two stages.

Suppose first that we fix the flow field, i.e. temporarily assume that $\phi(x, y)$ is known. We then seek a surface $y = \eta(x)$ upon which both $E(x, \eta(x)) = 0$ and $P(x, \eta(x)) = 0$. For a general $\phi(x, y)$ this is impossible; we can always find separately ("streamlines") $E = 0$ or ("isobars") $P = 0$, but these surfaces will not in general coincide. If they did, we would have solved our problem!

The streamlines can be found by a Newton iteration $\eta_0 \to \eta_0 + \eta_1$, where

$$\eta_1 = -\frac{E(x, \eta_0)}{E_y(x, \eta_0)} \tag{5}$$

and the isobars by

$$\eta_1 = -\frac{P(x, \eta_0)}{P_y(x, \eta_0)} \tag{6}$$

where $y = \eta_0$ is a known approximation to the required free surface. These two distinct surfaces will only coincide if

$$\frac{E(x, \eta_0)}{E_y(x, \eta_0)} = \frac{P(x, \eta_0)}{P_y(x, \eta_0)} \tag{7}$$

and this is the required *single* nonlinear boundary condition which must be satisfied on the *fixed* boundary surface $y = \eta_0(x)$. Once a flow satisfying (7) is determined, either (5) or (6) can be used to update the free surface, in a quadratically convergent iteration procedure.

The second stage of the solution process is to also use a Newton iteration to solve for a flow $\phi(x, y)$ subject to (7) on the (temporarily assumed known) surface $y = \eta_0(x)$. We now write $\phi = \phi_0 + \phi_1$ where $\phi_0$ is a current guess, and $\phi_1$ a correction to that guess. Then

$$E \approx E^0 + E'\phi_1 + O(\phi_1)^2 \tag{8}$$

where $E^0$ is the residual at the current guess, and $E'$ is a linear differential operator acting on $\phi_1$ whose coefficients depend on the current guess $\phi_0$. A similar equation holds for $P$.

Since $E$ and $P$ themselves can be assumed small (if we are sufficiently close to a converged solution) but the derivatives $E_y, P_y$ in the denominators of the boundary condition (7) are not necessarily small, it is consistent to use "old" values for the latter, while correcting the former using (8). Thus (7) is replaced by

$$\frac{E^0 + E'\phi_1}{E^0_y} = \frac{P^0 + P'\phi_1}{P^0_y} \tag{9}$$

This is a *linear* boundary condition for $\phi_1(x, y)$, to be applied on the *known* boundary $y = \eta_0(x)$, all superscript "0" quantities being evaluated on that boundary using the current guess potential $\phi_0(x, y)$.

In practice, for the two-dimensional free-surface problems of interest in the present paper, the various coefficients in (9) are straightforward to evaluate. For example, if we use the

Bernoulli equation with $P = -p/\rho$, and assume that $P = 0$ on the far upstream free surface $y = 0$ to eliminate the Bernoulli constant, we can write

$$P = gy + \frac{1}{2}\phi_x^2 + \frac{1}{2}\phi_y^2 - \frac{1}{2}U^2, \tag{10}$$

where $\rho$ is the fluid density, and $g$ is the acceleration due to gravity. Then

$$P'\phi_1 = \phi_{0x}\phi_{1x} + \phi_{0y}\phi_{1y} \tag{11}$$

and

$$P_y^0 = g + \phi_{0x}\phi_{0xy} + \phi_{0y}\phi_{0yy} \tag{12}$$

If $E$ is taken as the streamfunction, the coefficients for $E$ are in principle even easier to evaluate than those for $P$. However, we prefer not to use the streamfunction, in order that the numerical methods carry over easily to three dimensions. We could of course use for $E$ a measure of the actual normal component of velocity as specified in (2), but this presents some problems since it depends on the slope $\eta'(x)$ of the free surface. Instead we set

$$E(x,y) = \phi_x^2\phi_{xx} + 2\phi_x\phi_y\phi_{xy} + \phi_y^2\phi_{yy} + g\phi_y \tag{13}$$

The condition $E(x,\eta(x)) = 0$ is a "combined" kinematic-dynamic condition with the advantage that explicit dependence on $\eta$ has been formally eliminated (Newman 1977, p.247). The corresponding expressions for $E'$ and $E_y^0$ are straightforward to write down; note that the latter will involve up to third partial derivatives of $\phi$.

The final boundary condition (9) is then a fully-consistent updating condition, that allows us to move from one iteration to the next, being a linear condition applied on the previous free surface. It incorporates both direct perturbations to $\phi$ as well as what are sometimes (Raven 1992) called "transfer terms" expressing the contribution to the update from evaluation of the flow at the new rather than the old free surface. Only with all such terms included can the iteration converge quadratically. This boundary condition (9) is very complicated when all terms are written out (c.f. Jensen et al 1986), but its structure is best seen by leaving it in the form (9).

## 3. Stokes Waves

In part as a preliminary test of the numerical method, we have computed pure deep-water Stokes waves. That is, we assume periodicity with respect to $x$, and represent the flow in one half-wavelength by discrete sources above the free surface. The velocity potential for a line source at $(X,Y)$ between equipotential vertical boundaries at $x = 0$ and $x = \lambda/2$ can be written

$$\Phi_S(x,y;X,Y) = \Phi_0(x-X, y-Y) - \Phi_0(x+X, y-Y) \tag{14}$$

where

$$\Phi_0(x,y) = \log\left[\sin^2\frac{\pi}{\lambda}x + \sinh^2\frac{\pi}{\lambda}y\right] \tag{15}$$

If we therefore write

$$\phi(x,y) = Ux + \sum_{j=1}^{n}\sigma_j\Phi_S(x,y;X_j,Y_j) \tag{16}$$

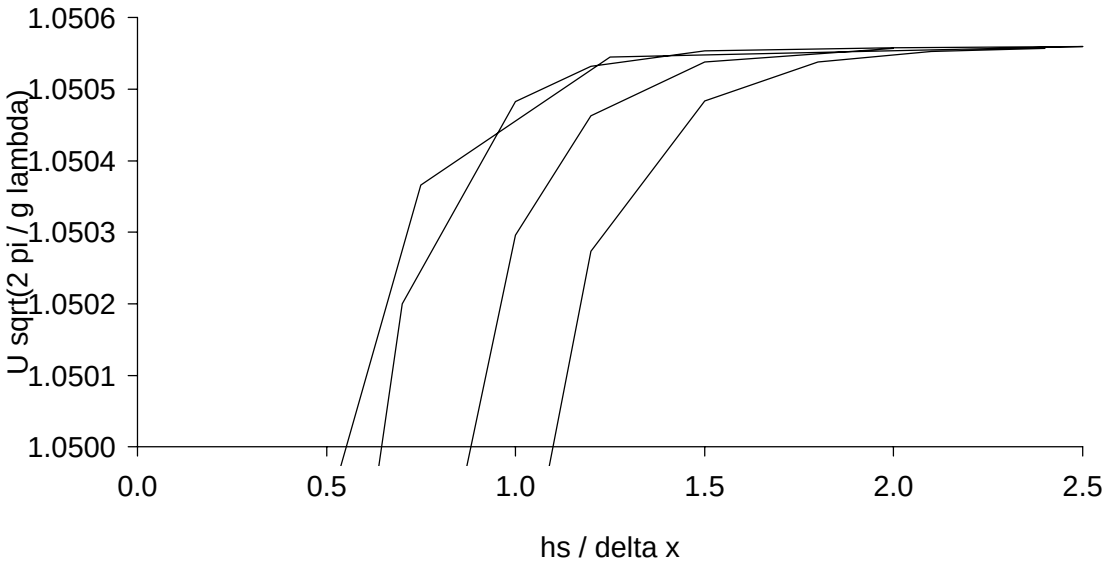


Figure 1: Wave speed versus desingularisation height, at various numbers $n$ of sources per half-wavelength, for Stokes waves with steepness 0.1 .

then this potential satisfies the required periodicity conditions (essentially that the vertical velocity component is zero) at two stations $x = 0, \lambda/2$ a half-wavelength apart.

Our task is to choose the vector of unknown source strengths $\{\sigma_j\}$ so that the kinematic and dynamic free surface conditions are satisfied on a free surface $y = \eta(x)$. This surface is also unknown, and is also specified by a vector consisting of some discrete sample of values $\{\eta_j\}$. An iteration procedure essentially equivalent to that described earlier was used to make this choice in a quadratically converging manner. It is convenient to fix the wavelength $\lambda$ and to allow the wavespeed (effectively via the gravity constant $g$) to be an unknown together with $\{\sigma_j\}$ and $\{\eta_j\}$. One small difference from the submerged-body problem is that we can no longer assume that the Bernoulli constant is zero, and hence must write the dynamic condition as $P =$ constant, with $P(x, y)$ as defined by (10), and the constant to be determined.

The location $(X_j, Y_j)$ of the sources is arbitrary, so long as it is above the free surface. Although other choices were tried, including placing the sources on a curved surface at a constant distance above the free surface, it was found that (even for very steep waves approaching the highest possible), placing the sources on a horizontal plane a fixed distance $h_s$ above the crest of the wave was adequate. Uniform spacing of the sources was also found to be adequate. In practice, the $n$ sources were placed vertically above the midpoints of $n$ segments into which the half-wavelength region was divided. Collocation occurred at the $n+1$ ends of these segments, thus giving $2n+2$ equations. The $2n+2$ unknowns are the $n$ sources, the $n$ free-surface heights at the segment ends (only $n$ because the trough-to-crest height is specified), the gravity constant $g$ and the value of the Bernoulli constant.

Some experimentation was carried out on the optimal choice of the source height $h_s$. Figure 1 shows results for a moderate wave with steepness 0.1, and Figure 2 for a highly-nonlinear wave with steepness 0.1375; the maximum steepness of a Stokes wave is 0.1411 (Schwartz 1974).

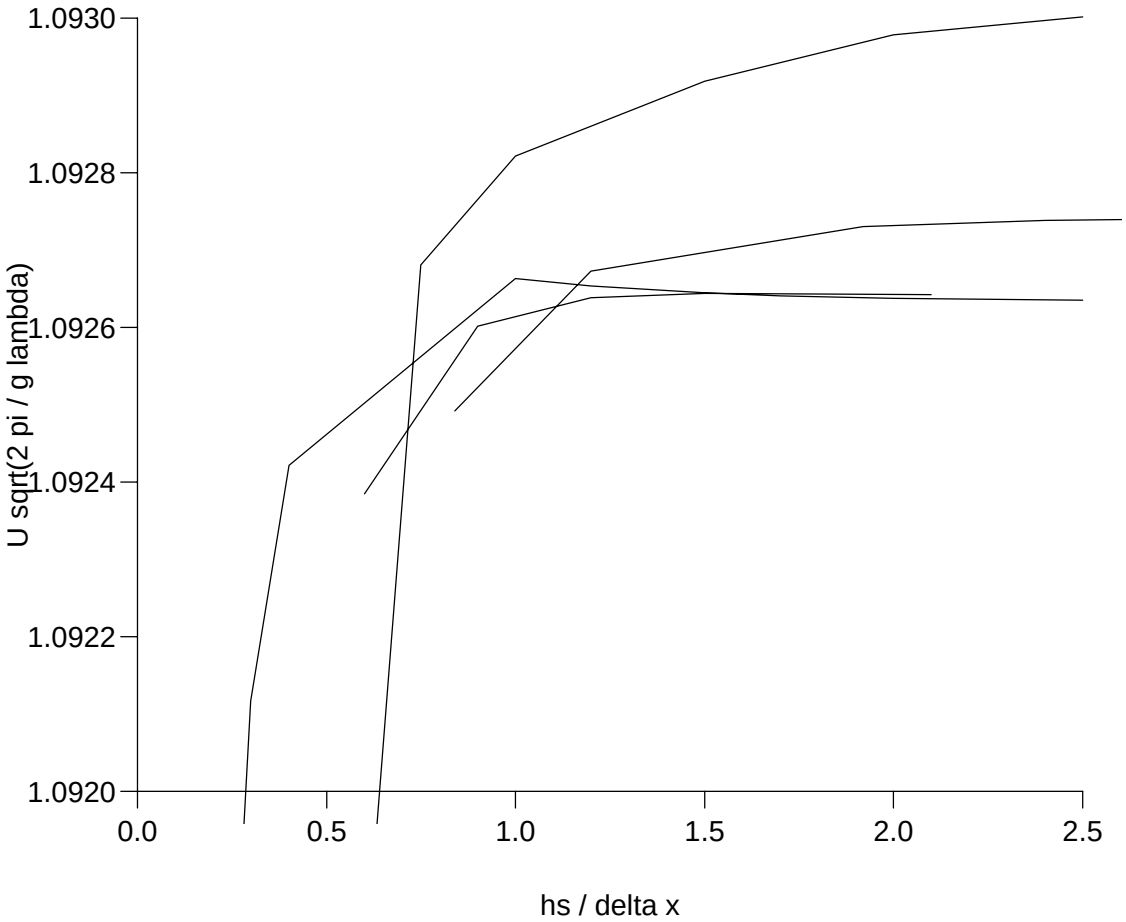


Figure 2: Wave speed versus desingularisation height, at various numbers $n$ of sources per half-wavelength, for Stokes waves with steepness 0.1375 .

The horizontal axis for these curves is the ratio between $h_s$ and the horizontal grid spacing $\Delta x = \lambda/(2n)$. The vertical axis is the non-dimensional wave speed or Froude number based on wavenumber $U\sqrt{2\pi/(g\lambda)}$, which takes a unit value for small waves, and reaches a maximum of 1.09295 at a steepness of 0.1388 (Cokelet 1977).

The general conclusion is that $h_s$ should be at least $\Delta x$, with some preference for about two to three times $\Delta x$. Little further improvement occurs beyond $h_s \approx 3\Delta x$. The iteration procedure sometimes fails to converge when $h_s$ is too large, and one minor disadvantage of the horizontal-plane location of the sources is that this can happen at the troughs even when the sources at the crests are sufficiently close.

However, such difficulties occur only for very high waves and large $n$ (small $\Delta x$). Figures 1 and 2 also indicate the extraordinarily rapid rate of convergence as $n$ increases. At steepness 0.1, as few as 12 sources per wavelength ($n = 6$) yields the full 6-figure accuracy of Schwartz's (1974) value 1.05056 for the wave speed. Even at steepness 0.1375, $n = 15$ is adequate for agreement with a 6-figure value 1.09264 obtainable from results of Cokelet (1977).

Although no serious attempt was made to push the present method to its limits, well-converged results were obtained up to a steepness of 0.1401. Placing the sources on a curved surface improved this only to 0.1404; if results closer to the highest wave, of steepness 0.1411, were needed, further improvements could possibly be effected by use of a non-uniform source spacing, concentrating sources near the crest.

## 4. Flow About Submerged Bodies

As our eventual intention is to develop a program which solves three-dimensional surface-piercing problems (e.g. for ships moving on the surface of the water) the code used to solve the current problem has been kept in a form that will enable this transition to be made easily. Consequently, the code is suitable for solving the two-dimensional problem for arbitrarily shaped bodies. The body need only be represented by a collection of points. However, for the results given in this paper we have restricted ourselves to the flow about a circular cylinder.

The potential for the flow is decomposed into three components. The first component represents the uniform stream of velocity $U$. The second component induces circulation $2\pi\kappa$ around the body, and can be taken to be a line vortex of strength $\kappa$ placed anywhere inside the body plus its reversed image placed anywhere above the free surface. The final component is that of the disturbance $\Phi$ created by the body. Thus we write the total potential as

$$\phi(x, y) = Ux + \kappa\,(\theta_1 - \theta_2) + \Phi(x, y). \tag{17}$$

Here $\theta_1$ and $\theta_2$ are the angles to the positive $x$-axis made by the lines joining the vortex and its image to a general field point $(x, y)$.

The disturbance potential $\Phi$ can be generated by a distribution of singularities either on the surface or else external to the fluid ("desingularised" in the terminology of Cao et al 1991). We choose to use the desingularised approach, and also choose (with Cao et al 1991) to use isolated two-dimensional point sources for the singularities, rather than smoothed-out sources over panels. This leads to simplifications in both analytic and numerical

evaluations of the potential, relative to formulations where the sources are distributed over panels on the boundary. Thus we write

$$\Phi = \sum_{j=1}^{n} \frac{\sigma_j}{2\pi} \log r_{ij} \tag{18}$$

where $r_{ij}$ is the distance between the source labeled $j$ and the field point of interest labeled $i$. Thus we are using a distribution of sources of strengths $\sigma_j$ which may lie anywhere within the body or above the free surface. Derivatives of the potential can easily be computed from similar expressions as all of the required information is known explicitly. Consequently, all boundary conditions are implemented directly from their analytic expressions which avoids the introduction of errors due to difference schemes.

As has been discussed in Section 2.1, the radiation condition must enforce the physical reality of no waves existing upstream, and the necessary two conditions could be any two conditions that cannot be satisfied simultaneously by a wave. We found that enforcing a requirement that the vertical component of velocity decays in proportion to the inverse cube of distance (equivalent to free-surface elevation decaying as the inverse square), at two different but nearby locations sufficiently far upstream, was successful in eliminating upstream waves. Specifically, our radiation condition was

$$\frac{\partial^2 \Phi}{\partial x \partial y} + \frac{3}{x} \frac{\partial \Phi}{\partial y} = 0 \tag{19}$$

which was enforced at two points near the beginning of the computational domain (we chose the first and fifth).

### 4.1 Forces acting on the submerged body

We have evaluated the force on the body by two different methods. The first is by integration of pressure over the body surface, and the second is via the use of the Lagally theorem. In the pressure integration method, the pressure is evaluated via Bernoulli's equation at collocation points on the body, and then the integral

$$\mathbf{F} = -\oint_B p \, d\mathbf{s} \tag{20}$$

is approximated by the rectangle rule. For integration about a closed path, this is equivalent to the trapezoidal rule. Note that although for the special case of a circular cylinder we could make much better approximations, in general we will not have an analytic expression for the body shape and so will be more reliant on simple approximations. This method of pressure integration is quite simple to implement but is slightly susceptible to errors within the integration procedure.

Alternatively, as the potential field is described by a distribution of singularities (in our case they are line sources and line vortices) the force lends itself easily to evaluation by Lagally's theorem. Milne-Thomson (1968) gives a derivation of this theorem via the residue theorem. If we define $X_F$ and $Y_F$ to be the components of force in the $x$ and $y$ directions respectively, then

$$\overline{F} = X_F - iY_F \tag{21}$$

is the complex force and the Lagally theorem states that the force $\overline{F}_{S_j}$ on a body due to a single source $j$ external to the body is given by

$$\overline{F}_{S_j} = 2\pi\rho\sigma_j \overline{q}_j, \tag{22}$$

and

$$\overline{q}_j = u_j - iv_j \tag{23}$$

is the velocity induced at the location of the source by all other singularities (including vortices) except the source $j$. The total force due to a distribution of sources is then the sum of the forces due to individual *external* sources, ie.

$$\overline{F}_S = \sum_j \overline{F}_{S_j}. \tag{24}$$

Similarly, the force on the body due to a single external vortex $j$ of strength $\kappa_j$ is given by

$$\overline{F}_{V_j} = -2\pi i \rho \kappa_j \overline{q}_j. \tag{25}$$

These can also be summed over *external* vortices to give the total force due to a distribution of vortex points

$$\overline{F}_V = \sum_j \overline{F}_{V_j}. \tag{26}$$

The final component of force is due to the circulation about the cylinder (produced by the vortex within the body) and is given by the Kutta-Joukowski theorem

$$\overline{F}_\kappa = 2\pi i \rho U \kappa, \tag{27}$$

where $\kappa$ is the strength of the vortex within the body.

The total force on the body due to the distribution of line sources and the two vortex points is then just the sum of these three components, and is simple to evaluate. In fact, certain other simplifications can be made because many of the terms required above can be shown to cancel. This reduces the amount of computational effort required to evaluate the total force on the body.

The two methods of force calculation are found to be in good agreement (typically to 4 or 5 significant figures), but as the integration method requires the integral to be approximated by a sum, it is considered to be the inferior method of the two. Consequently, all results stated within this paper have been calculated by the Lagally theorem.

### 4.2 Wave resistance for a submerged circular cylinder without circulation

As an initial exercise we sought verification of consistency of our program with existing approximate theories. Tuck (1965) investigated the wave resistance of a submerged circular cylinder by a consistent second-order expansion in the small parameter $a/h$, where $a$ is the radius of the cylinder and $h$ the depth of its centre beneath the undisturbed free surface, and compared the results to the first-order theory. For comparison with these approximations we have produced results for a variety of $a/h$ ratios and Froude numbers

$$F = \frac{U}{\sqrt{gh}}, \tag{28}$$

based on submergence depth $h$.

In Figure 3 we show a typical example of the distribution of sources above the free surface and within the submerged body, the body itself, and the converged free-surface solution for

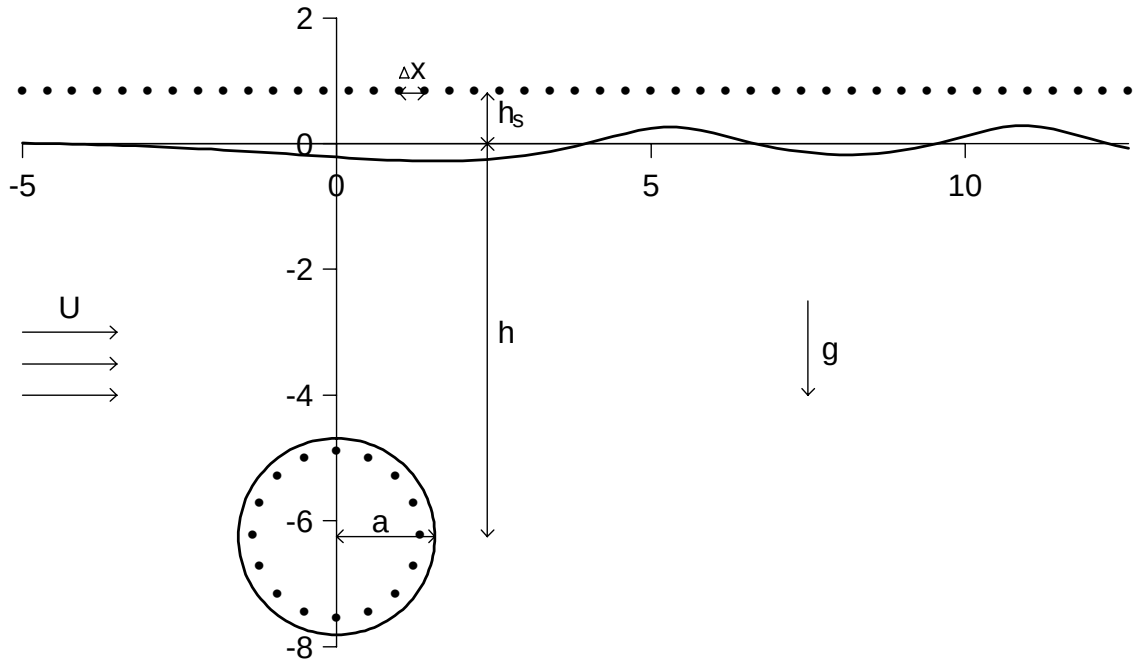


Figure 3: An example defining parameters used in the solution process, and showing the location of sources external to the fluid and within the submerged body.

such a task. In general, our computational domain was the $x$-interval $(-30, 30)$, with 301 sources distributed along the plane $y = 0.8$ at equal intervals of 0.2. As was consistent with our findings for the Stokes waves, distributing the sources along a plane at a fixed distance above the free surface was satisfactory, and is the preferred method considering the ease with which this can be coded. The 299 free surface collocation points were located directly beneath each of the source points (with the exception of the two external source points) and initially along the $x$-axis, and are allowed to rise or fall with each iteration to achieve the converged free surface. The cylindrical body was centered about the point $(0, -h)$ and was represented by 128 body collocation points, on equally spaced rays. A source point was also located on each of these rays but buried within the cylinder at a radius of $0.85a$. The free stream velocity $U$ and gravity $g$ were kept constant at 1, with the Froude number $F$ being varied by its dependence on $h$. In effect then, we are working with approximately 30 collocation points per wavelength and with a $h_s/\Delta x$ ratio of 4. Experiments for this problem similar to those discussed in Section 3 showed that operating with more than 15 points per wavelength and with a $h_s/\Delta x$ ratio greater than 2 would produce accurate results.

Figure 4 shows these results of these computations in graphical form. The vertical axis is given in terms of the dimensionless quantity

$$\bar{R} = \frac{X_F h^2}{\pi \rho g a^4}. \tag{29}$$

With the wave resistance expressed in this form, the first-order linear theory consists of a universal curve versus Froude number, specifically the graph of

$$\bar{R} = 4\pi F^{-4} e^{-2/F^2} \tag{30}$$

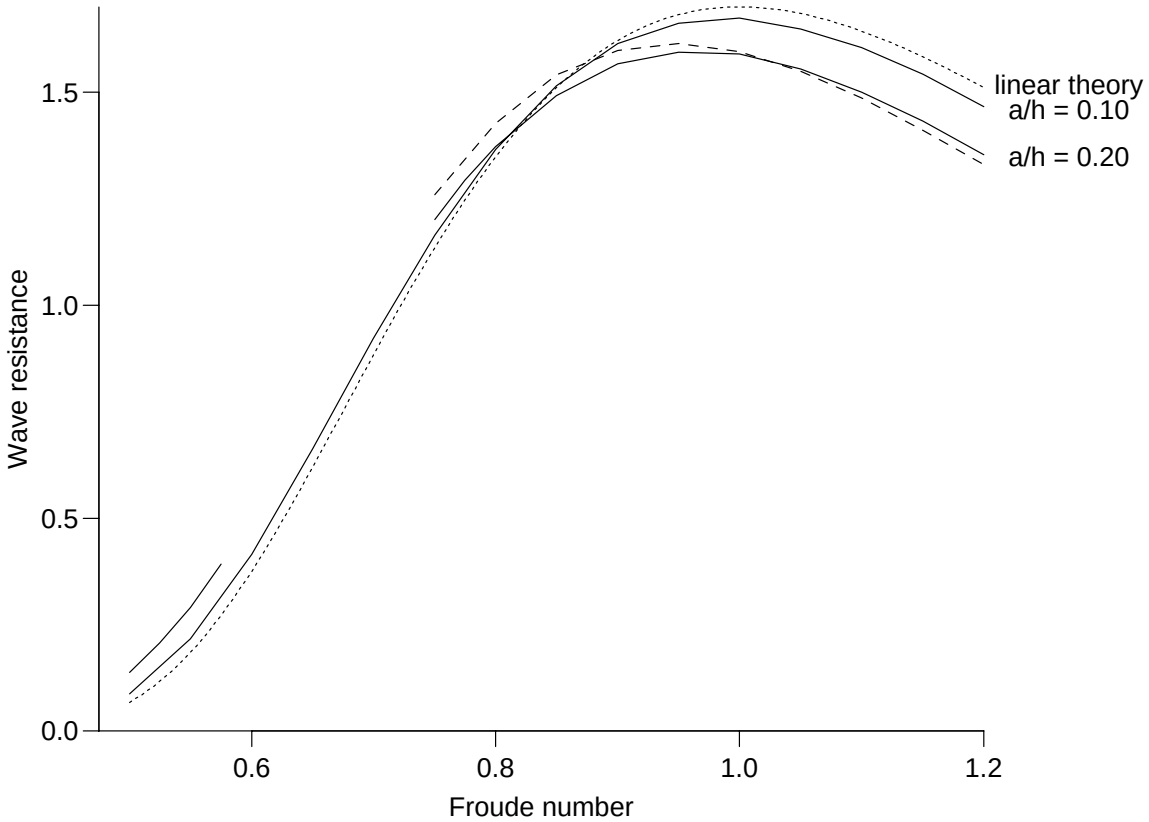


Figure 4: Wave resistance for submerged circular cylinders without circulation. Solid lines are our results at $a/h = 0.1$ and $a/h = 0.2$. Dotted curve is first-order linear theory (indpendent of $a/h$), dashed curve is second-order linear theory at $a/h = 0.2$.

and is independent of the radius-to-depth ratio, but is valid only when that ratio is small. The consistent second-order approximation requires a different curve for each radius-to-depth ratio, the difference between each such curve being proportional to the square of $a/h$ at fixed $F$.

As can be seen from Figure 4, our results are in close agreement with the linear theory for sufficiently small radius. In fact our results are graphically indistinguishable from the second-order theory for $a/h = 0.1$, and the departure from the first-order theory still shows good correlation with the second-order theory for larger cylinder radii. However, for sufficiently large disturbances, including $a/h = 0.2$, our code fails to converge for some Froude numbers, and we have left a break in the curve for $a/h = 0.2$ in Figure 4 to indicate that. Even for $a/h = 0.2$, though, there is still reasonable agreement with the second-order theory for those Froude numbers at which we can produce results.

### 4.3 On the existence of a steady potential solution

For large enough disturbances, we would expect that the physical solution to the problem would produce a breaking wave. Similarly, we would question if such cases could be modelled by a potential flow method, or indeed a steady method. As the non-linearity of the disturbance increases, it is more difficult to obtain a solution, and whether this is due

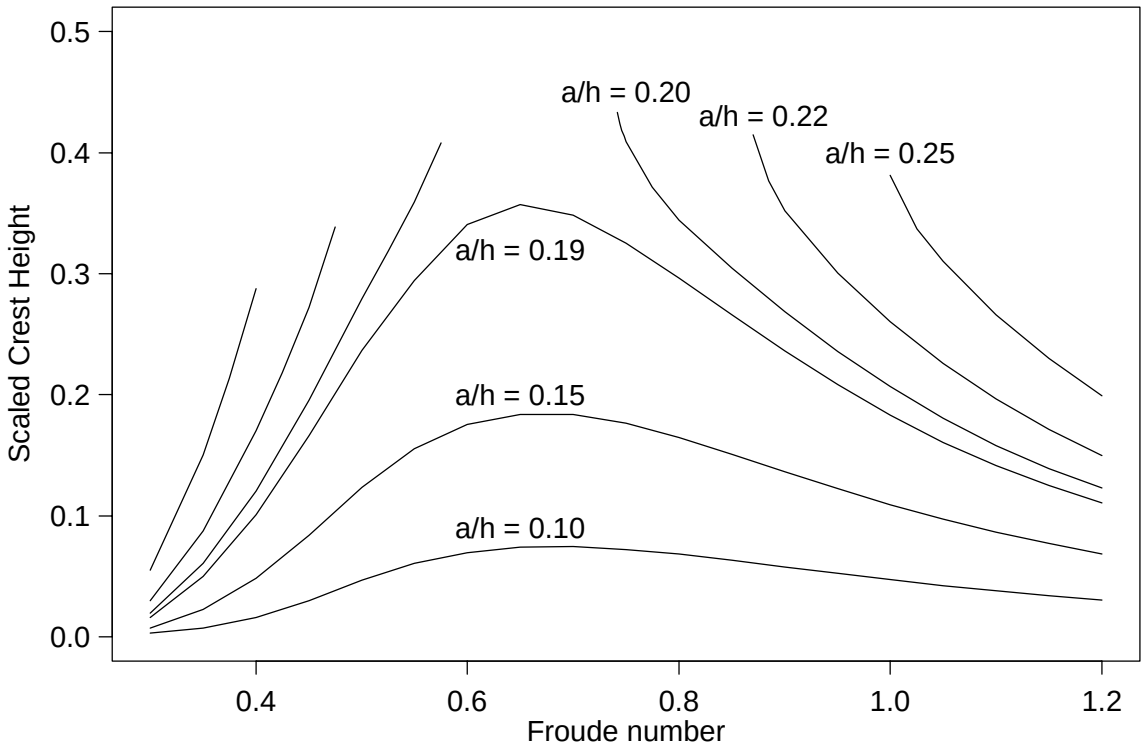


Figure 5: Scaled height of the highest point on the free surface, plotted as a function of Froude number, for various values of $a/h$.

to the non-existence of a steady potential solution or else due to some other complication such as a numerical artefact is not always clear. Figure 5 is a plot versus Froude number of the height of the first crest, which is usually the highest point of the free surface, for various values of $a/h$. All of these results have been scaled with respect to the lengthscale $U^2/g$, so that the highest possible free-surface point has the stagnation height $U^2/(2g)$ which scales to 0.5. It is important to note that there may not exist a steady potential solution for which the crest actually reaches the stagnation height. The quantity plotted in Figure 5 is then a measure of the extent of non-linearity, with 0.5 corresponding to an upperbound.

For the smaller cylinder sizes, with $a/h = 0.10$, 0.15 and 0.19, we can see that there are always steady solutions, throughout the entire range of Froude numbers. However, for the larger disturbers with $a/h$ of 0.20, 0.22 and 0.25, it is clear that the wave height is increasing rapidly near some particular Froude numbers, and there is a range of Froude numbers for which our program does not produce any solution. The behaviour of the graphs in Figure 5, in particular, the fact that they are approaching the upperbound height 0.5 at the edges of this range, suggests strongly that no steady potential solutions exist in this range. For $a/h = 0.22$, on this basis we estimate that no solution exists for Froude numbers between 0.50 and 0.85. For the even larger cylinder with $a/h = 0.25$, the range of Froude numbers would possibly be as wide as 0.45 to 0.95.

Another point to note is that it is difficult to compute waves by our program with a maximum scaled height greater than about 0.430, which corresponds to a (far-downstream) wave steepness of approximately 0.114. In fact, to produce results with a maximum scaled

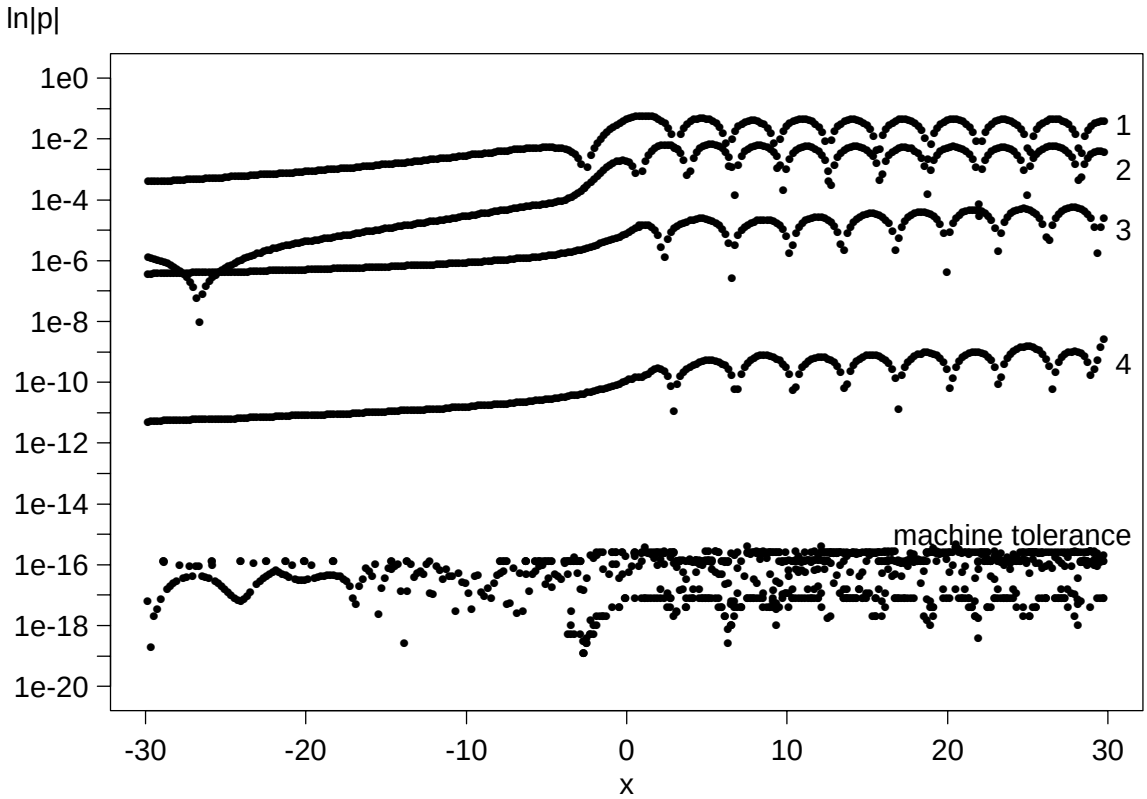


Figure 6: Residual error in the dynamic free surface condition showing quadratic convergence behaviour. $a/h = 0.1$, $F = 0.5$

height larger than approximately 0.375 requires care and considerable computational effort, whereas for smaller waves the results can be produced to within tolerances of $10^{-8}$ in just 6 or 7 iterations. Figure 6 shows clearly the quadratic convergence of the method, to the extent that for this reasonably linear case the residual error in the dynamic free surface condition is dominated by the machine tolerance after only the fifth iteration.

One of the main reasons for divergence is due to the non-linear effect of wavelength reduction, which causes the early approximations in our iteration scheme to have crests where the final converged solution will have troughs. The required correction is then larger, and this can lead to divergence. It should be noted that this change in wavelength is a "subharmonic perturbation" (Longuet-Higgins 1978) whose effect on pure Stokes waves is (weakly) unstable even for small waves, but strongly unstable for steepnesses greater than about 0.13, so we should not expect to be able to compute up to high steepnesses by the present method without fixing the wavelength, as was done in our own Stokes-wave computations.

Relaxing the amount by which the potential is perturbed at each iteration step can often delay this instability sufficiently for the iterations to settle down with the correct wavelength, although the quadratic rate of convergence of the process is then destroyed. Also, all of the results given here take the undisturbed plane free surface as the initial approximation. For significantly non-linear cases, using a closer approximation to the final free surface and potential (perhaps from the converged result of a similar case) could reduce the number of iterations required.

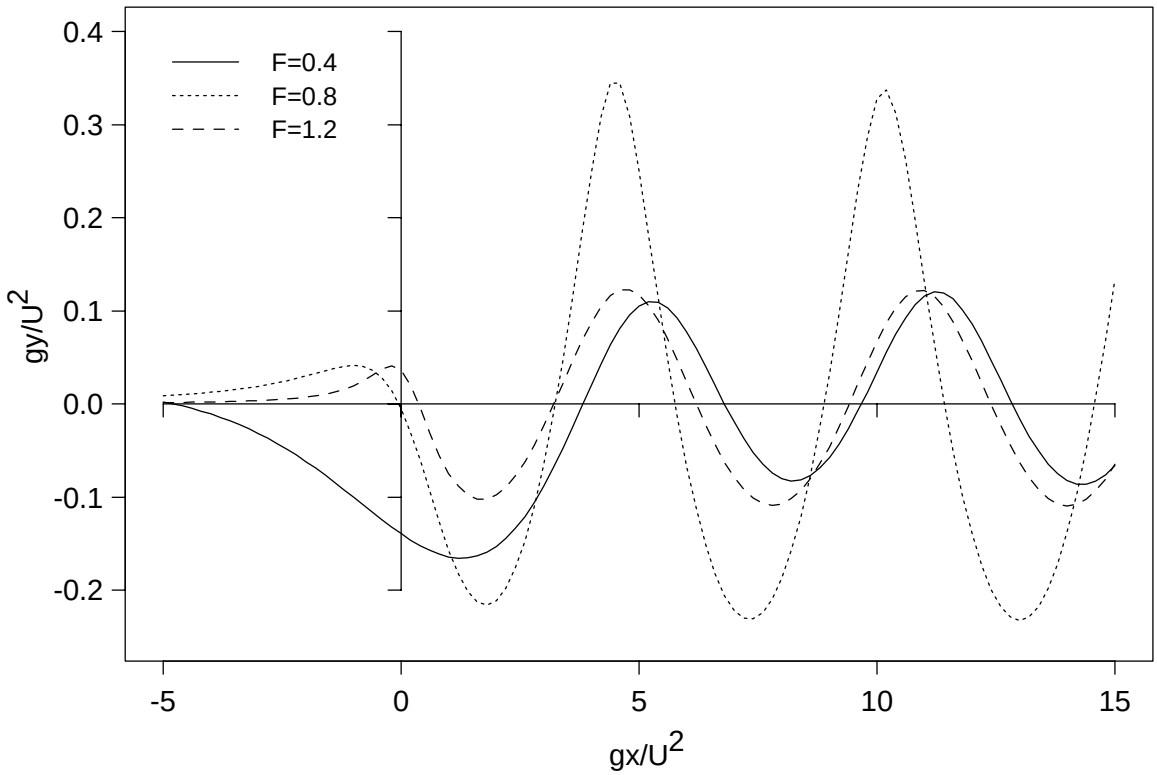


Figure 7: Examples of waves produced by the cylinder $a/h = 0.2$ at various Froude numbers.

For very steep waves, we do not have very good resolution near the peaks. We could improve upon this by decreasing the distance between neighbouring points, but this would necessitate the shifting of source points away from a plane above the wave to a shape that more closely follows the wave. This is expected to be only slightly more complicated, and will be incorporated if it proves to be necessary for the three dimensional case.

Figure 7 shows examples of the free-surface shape computed by our program at $a/h = 0.2$, for a low, medium and high value of the Froude number. Note that the highest waves are at the medium Froude number, and that these are significantly non-sinusoidal. Note also how the predominant local free-surface displacement ahead of the cylinder is a (strong) depression at low Froude numbers but this changes to a (weak) elevation at high Froude numbers.

As a final point, Figure 4 suggests that wave resistance would not be greatly affected for cases in which we cannot produce a solution. There is no evidence to show that the wave resistance would vary dramatically from that which could be expected from interpolation of these curves, at least not for those cases in which we have solutions except in a narrow band of Froude numbers.

### 4.4 Wave-making of submerged circular cylinders with circulation

Tuck and Tulin (1992) observed that the linear theory suggested that there exists a circulation about the submerged cylinder for which waves are not produced downstream, and hence the body feels zero wave resistance. They found that linear waves are totally

eliminated for a particular circulation $2\pi\kappa_0$ such that

$$\kappa_0 = a^2 g/U. \tag{31}$$

They also noted that for this circulation a force acting downwards of magnitude equal to twice the buoyancy was produced. No unsupported body could produce such a circulation.

The linear theory also indicates that as circulation is increased from zero to the critical value, the amplitude of the waves produced by the disturbance decreases linearly and becomes zero at $\kappa = \kappa_0$. If the circulation is increased further still, waves reappear and grow in amplitude but they have the opposite phase to those for which $\kappa < \kappa_0$. Crests now appear where there used to be troughs, and vice-versa. All of this occurs without any change in wavelength, and the only change in phase is a change of $\pi$ as the circulation passes through the critical value.

We have produced results for a variety of combinations of submergence depths and circulations. For cylinders of sufficiently small radius, our results are in agreement with the linear theory, and the phenomena mentioned above are observed (see Figure 8), which shows our computations for the very small cylinder $a/h = 0.02$. A local hump is produced on the free surface above the disturber, which grows in amplitude as the circulation is increased. Although this hump can be large in magnitude compared to the amplitude of the downstream waves, it is of a symmetric form, with the waves superimposed upon it. As a result, the submerged cylinder feels no drag due to this hump, the drag being due only to the energy radiation in the downstream waves, which are reduced by the circulation, so reducing the wave resistance. The local hump does however introduce a downforce proportional to the circulation.

Some interesting results are found for more strongly non-linear cases. In some cases, notably for relatively high Froude numbers the wave amplitude (and hence wave resistance) is dramatically reduced over a range of circulations from considerably less than $2\pi\kappa_0$ to considerably more. For example, Figure 9 gives our results for $a/h = 0.1333$ and $F = 1.0$. In other cases (for lower F values), waves could not be made to reappear at all when $\kappa$ is increased above $\kappa_0$. Figure 10 gives such results for $a/h = 0.1333$ and $F = 0.3651$. There was a gradual small phase shift associated with the increasing circulation. If the circulation is increased still further, the local hump grows in amplitude until it is so large that our program again fails to produce converged solutions, even though the far-downstream waves are quite small. This typically happens when the height of the local hump is 0.8–0.9 times the stagnation height. We are unsure of the existence of a solution in the cases where the program fails.

Of particular interest are the results for $\kappa = \frac{1}{2}\kappa_0$, as in this case the net lift on a massless body is close to zero according to the first-order linear theory. The downforce due to the circulation exactly cancels the buoyancy in that theory, and the only remaining effect is due to the free surface. Thus it is possible to have an unsupported cylinder which experiences a much lower wave resistance than it would without circulation. The linear theory suggests that the wave resistance at this circulation is one quarter of the wave resistance for the case of zero circulation. Our results show that in the more non-linear cases, and for Froude numbers approximately 0.5, the reduction in wave resistance can be substantially greater. Figure 11 shows the wave resistance for varying Froude number at a circulation of $\pi\kappa_0$ for the same $a/h$ values as in Figure 4. It also has an additional curve corresponding to the even larger disturber $a/h = 0.25$, for which converged solutions with circulation can be

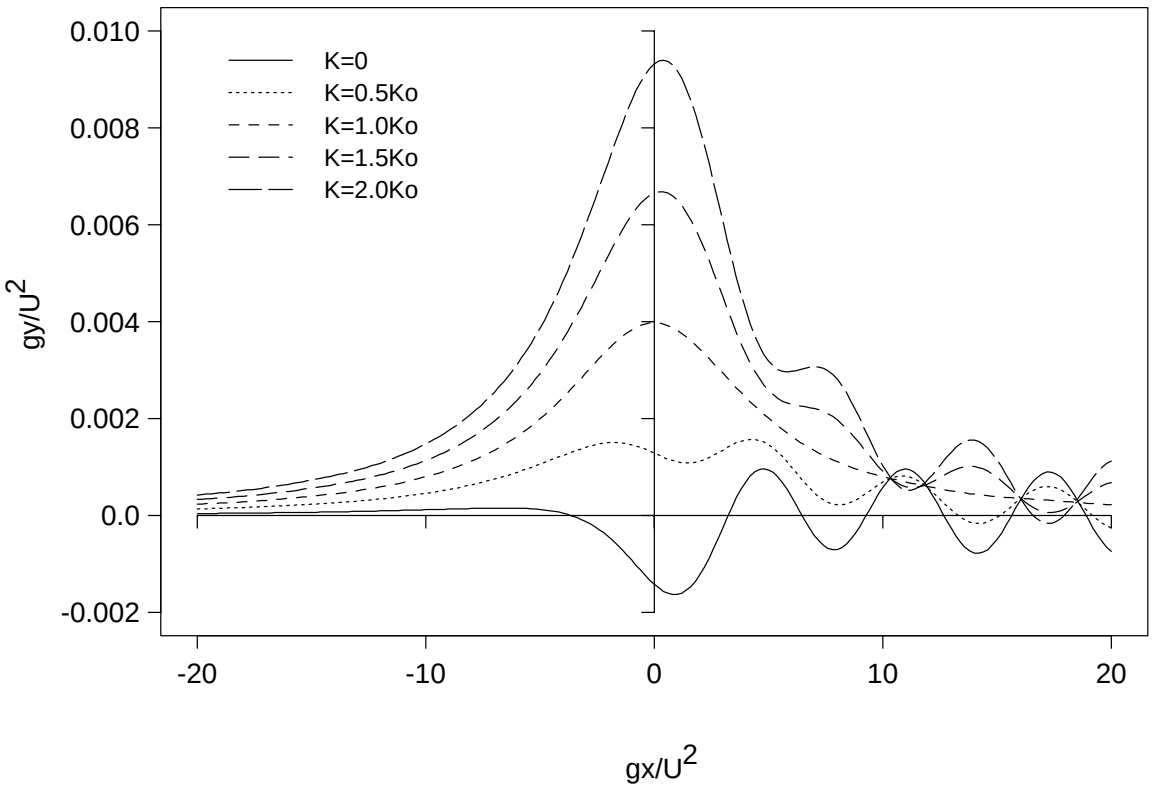


Figure 8: Almost linear ($a/h = 0.02$) waves produced by cylinders with differing circulations.

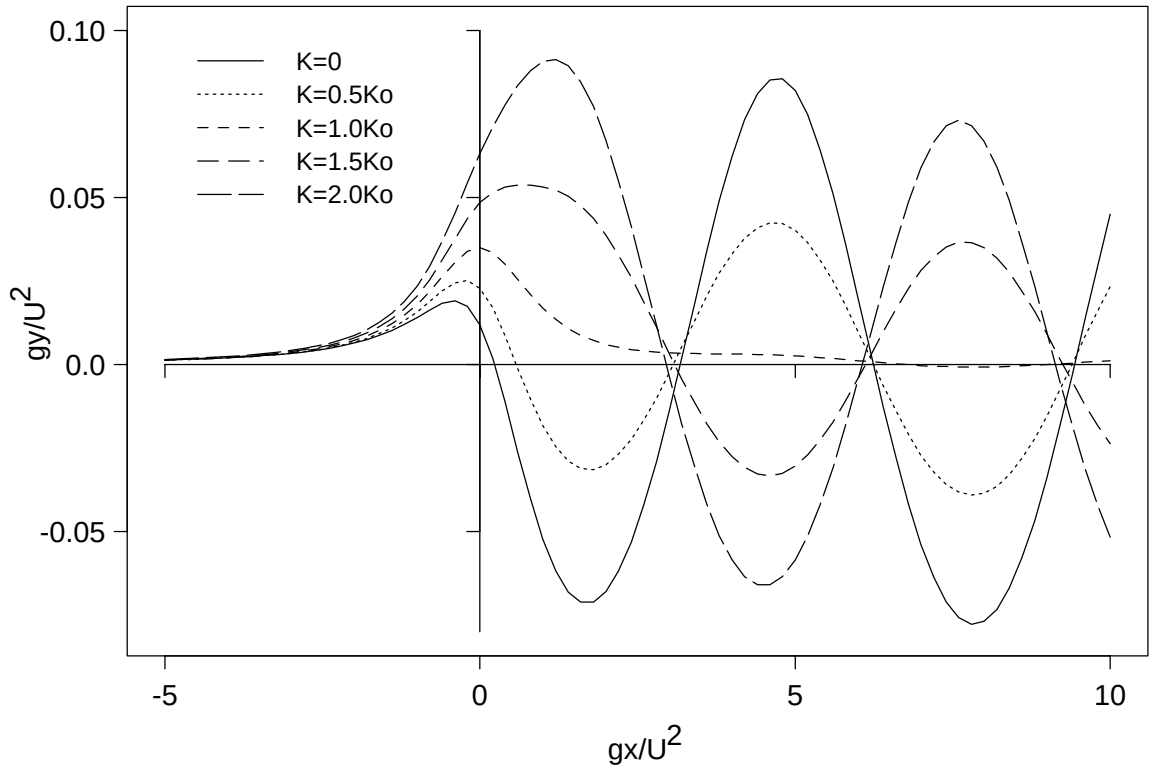


Figure 9: Non-linear waves produced by cylinders ($a/h = 0.1333$) with differing circulations at $F = 1.0$.

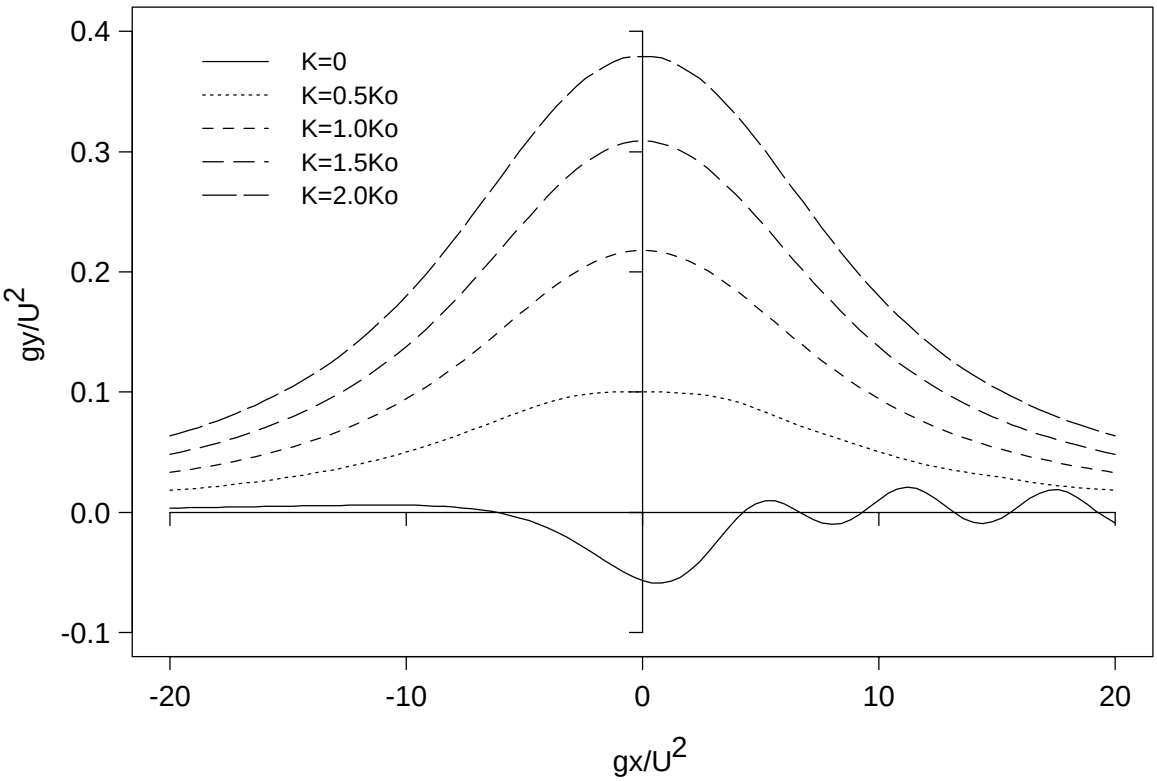


Figure 10: Non-linear waves produced by cylinders ($a/h = 0.1333$) with differing circulations at $F = 0.3651$.

obtained throughout the range of Froude numbers, whereas with zero circulation converged solutions do not always exist. The solid curves are our results at $a/h = 0.1, 0.2, 0.25$. The dotted curve is the first-order linear theory. Note that large disturbers at low Froude numbers have significantly lower wave resistances than predicted by the linear theory.

The wave resistance at the critical choice $\kappa = \kappa_0$ can be computed by the present program, but its magnitude is so small that the results are not significant. If the circulation is increased even further to $\kappa = \frac{3}{2}\kappa_0$, the linear theory predicts a wave resistance identical to that for $\kappa = \frac{1}{2}\kappa_0$. Figure 12 shows this result (dashed), compared to our nonlinear computations for various $a/h$ values. The nonlinear results seem to imply a much lower wave resistance than that for $\kappa = \frac{1}{2}\kappa_0$, especially at low Froude numbers.

With the lift expressed in terms of the non-dimensional quantity

$$\bar{L} = \frac{Y_F}{\pi \rho g a^2} \tag{32}$$

where the denominator is the buoyancy of the cylinder, linear theory predicts

$$\bar{L} = -a^2 \left[ 0.5h^{-3} + h^{-2} + 2h^{-1} - 2e^{-2h} \Re Ei^{-}(2h) \right] - 2\kappa/\kappa_0. \tag{33}$$

The terms not involving $\kappa$ are as in Tuck (1965), but in general if $\kappa \neq 0$ these terms are dominated by the last term involving the circulation. Hence, $\bar{L}$ is close to 0 in the absence of circulation, and close to $-1$ for $\kappa = \frac{1}{2}\kappa_0$.

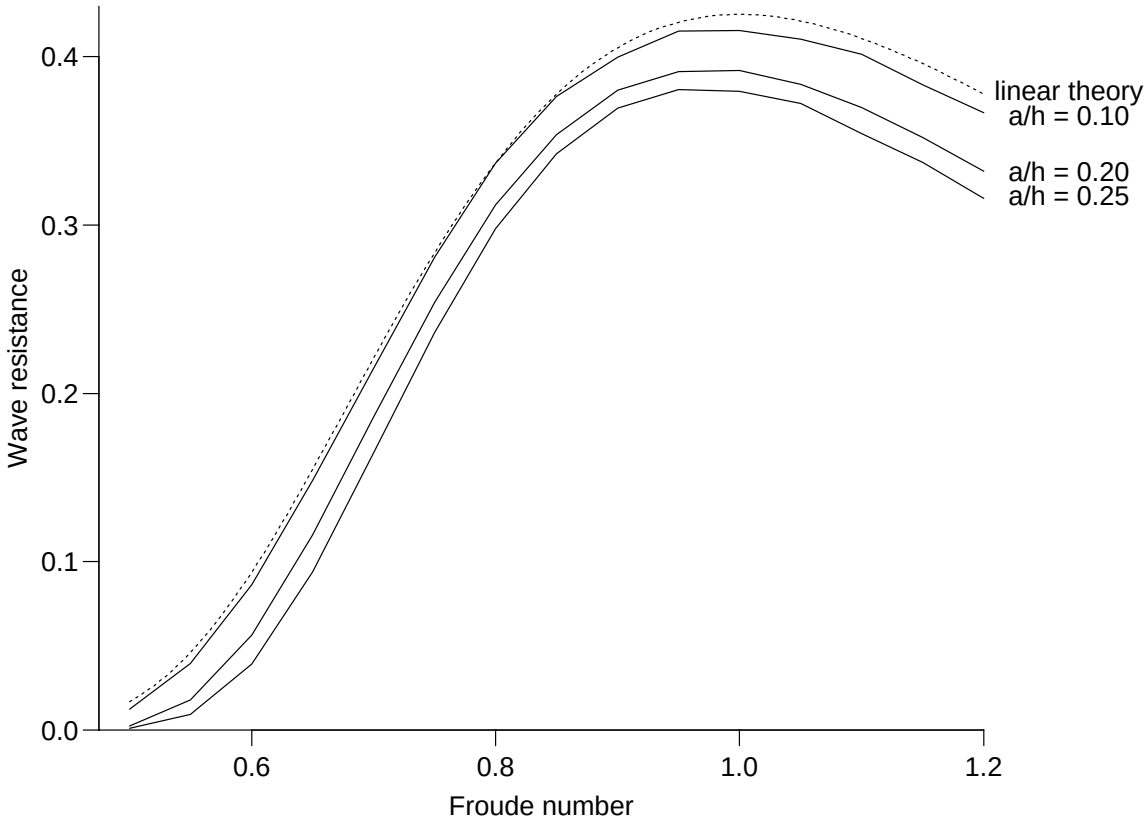


Figure 11: Wave resistance for submerged circular cylinders with circulation given by $\kappa = \frac{1}{2}\,\kappa_0$. Solid curves are our results at $a/h = 0.1, 0.2, 0.25$. Dotted curve is first-order linear theory.

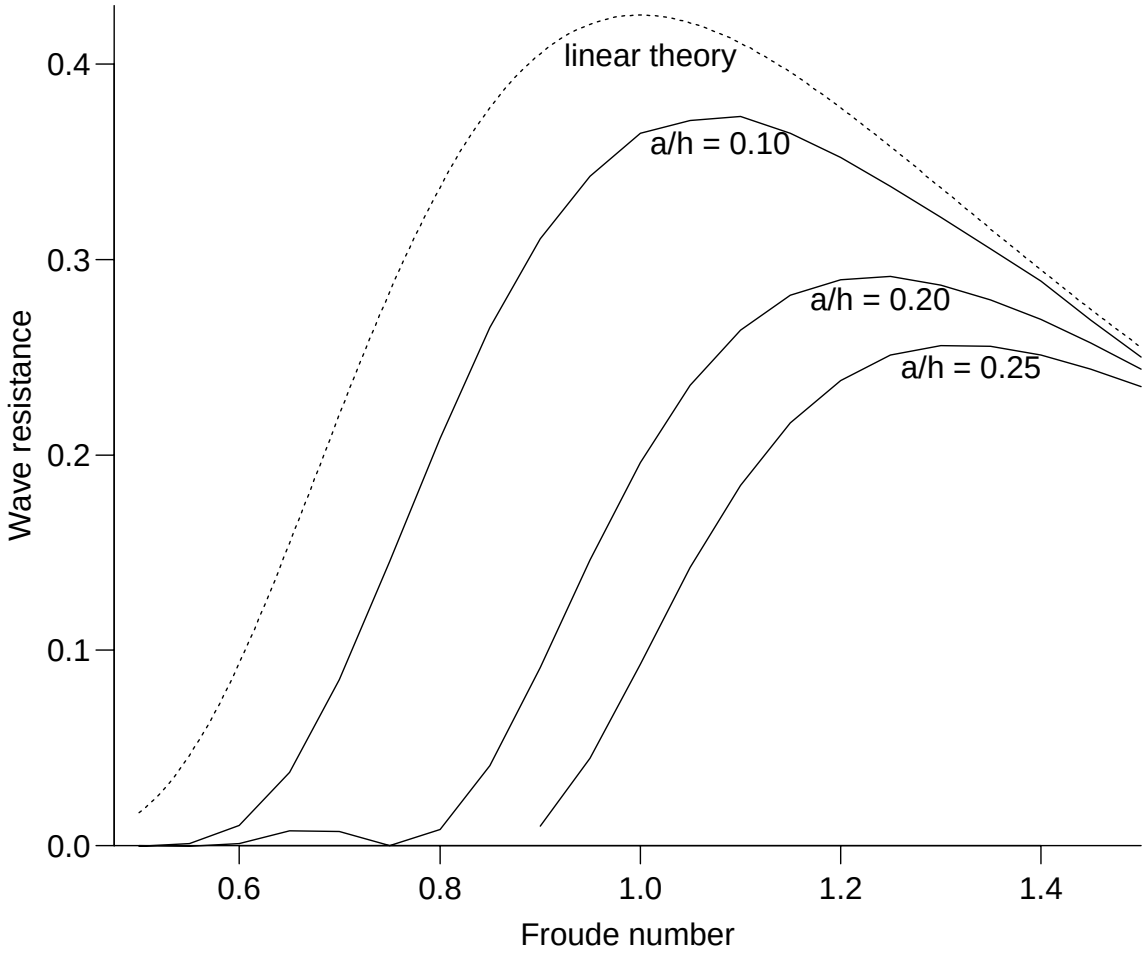


Figure 12: Wave resistance for submerged circular cylinders with circulation given by $\kappa = \frac{3}{2}\,\kappa_0$. Solid curves are our results at $a/h = 0.1, 0.2, 0.25$. Dotted curve is first-order linear theory.

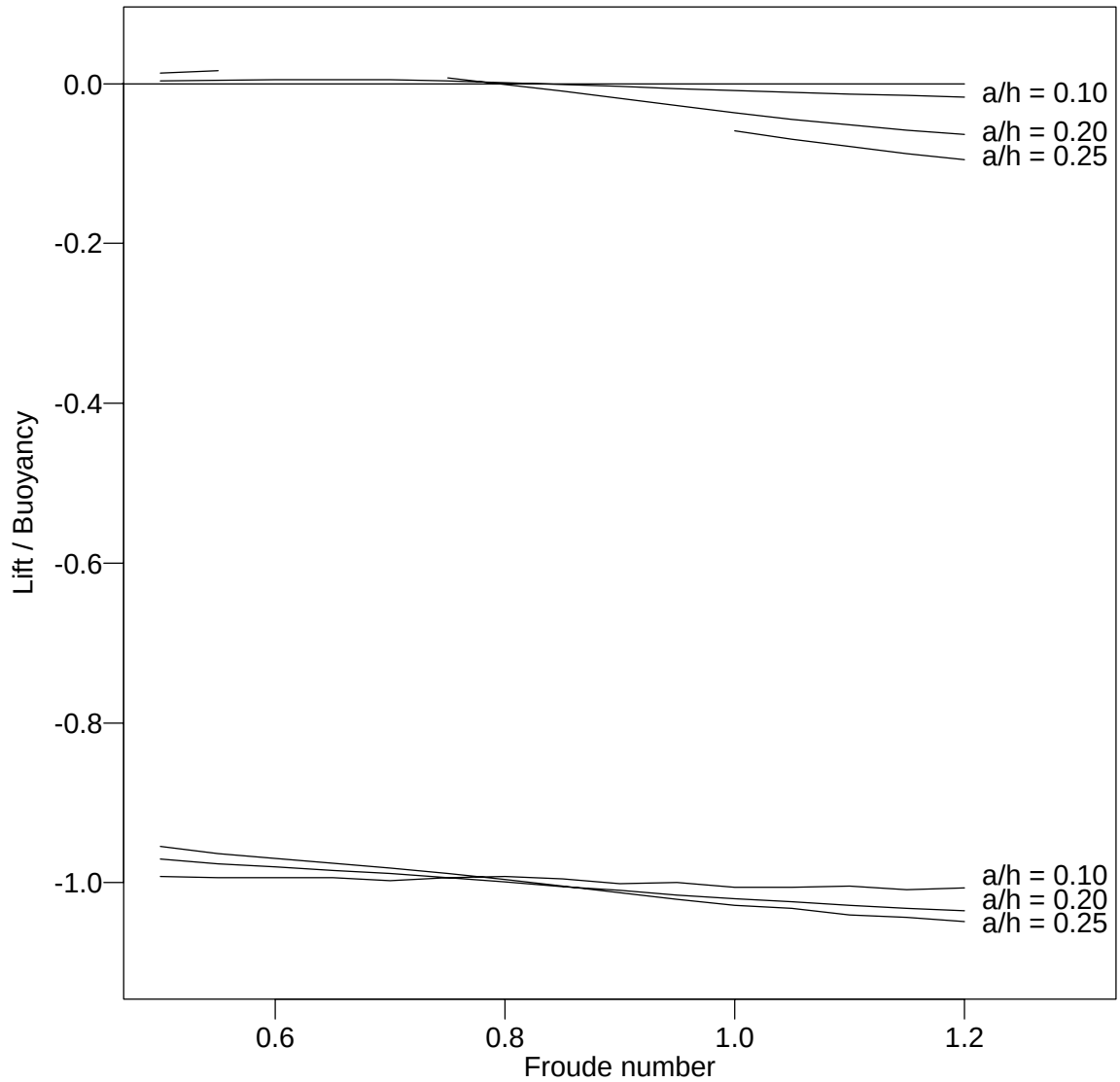


Figure 13: Lift for submerged circular cylinders without circulation and with circulation given by $\kappa = \frac{1}{2}\,\kappa_0$, $a/h = 0.1, 0.2, 0.25$.

Figure 13 displays the lift computed for the cases $a/h = 0.1, 0.2, 0.25$, for both of these values of circulation. Again, the results are consistent with linear theory for the sufficiently small disturber $a/h = 0.1$ and show the expected small variation for the more nonlinear cases.

There are (as linear theory predicts) values of circulation for which waves are eliminated and the wave resistance is zero. However, linear theory suggests that for any particular combination of radius, free-stream speed and gravitational acceleration, that value of circulation is unique. Non-linear effects modify this conclusion to the extent that there may exist a range of circulations for which waves are not produced. This range may well incorporate circulations for which an unsupported body need not be thrust downwards.

# References


CAO Y., SCHULTZ W.W. AND BECK, R.F. 1991 Three-dimensional desingularized boundary integral methods for potential problems. *Int. J. Num. Meth. Fluids* **12**, 785-803.

COKELET, E.D. 1977 Steep gravity waves in water of arbitrary uniform depth. *Phil. Trans. Roy. Soc. Lond. Ser. A* **286**, 183-230.

HAVELOCK, T.H. 1926 The method of images in some problems of surface waves. *Proc. Roy. Soc. Lond. Ser. A* **115**, 268.

JENSEN, G., MI, Z.X., AND SODING, H. 1986 Rankine source methods for numerical solutions of the steady wave resistance problem. *Proceedings*, 16th Symp. Naval Hydro., Berkeley, Calif.

LONGUET-HIGGINS, M. 1978 The instabilities of gravity waves of finite amplitude in deep water. II Subharmonics. *Proc. Roy. Soc. Lond. Ser. A* **360**, 489-505.

MILNE-THOMSON, L.M. 1968 *Theoretical Hydrodynamics, Fifth Edition.* MacMillan & Co Ltd., New York.

NEWMAN, J.N. 1977 *Marine Hydrodynamics.* MIT Press, Cambridge.

RAVEN H. 1992 A practical nonlinear method for calculating ship wavemaking and wave resistance. *Proceedings* 19th Symp. Naval Hydro., Seoul, Korea.

SCHWARTZ, L.W. 1974 Computer extension and analytic continuation of Stokes' expansion for gravity waves. *J. Fluid Mech.* **62**, 553-578.

TUCK, E.O. 1965 The effect of non-linearity at the free surface on flow past a submerged cylinder. *J. Fluid Mech.* **22**, 401-414.

TUCK, E.O. AND TULIN, M.P. 1992 Submerged bodies that do not generate waves. *Proceedings* 7th Int. Workshop on Water Waves and Floating Bodies, Val de Reuil, France.

WEHAUSEN, J.V. AND LAITONE, E.V. 1960 Surface waves. *Handbuch der Physik*, Vol. 9, S.Flugge, Ed., Springer-Verlag, Berlin.